# Lateral Confinement Needed to Suppress Softening of Concrete in Compression

Ferhun C. Caner[1]; and Zdeněk P. Bažant, F.ASCE[2]

**Abstract:** Suppression of softening in the load-deflection diagram of concrete-filled tubular columns and spiral columns is proposed to serve as a design criterion helping to avoid the size effect and explosive brittle character of collapse. To this end, the recently developed ''tube-squash'' tests, in which a short concrete-filled steel tube is squashed to about a half of its original length and allowed to bulge, are conducted with tubes of different wall thicknesses. A finite-strain finite element computer code with a microplane constitutive model is used to simulate the tests. After its verification and calibration by tests, the code is used to analyze nonbuckling concrete-filled tubular columns and spirally reinforced columns. It is found that softening in the load-deflection diagram can be fully suppressed only if the reinforcement ratio (ratio of the tube volume or spiral volume to the total volume of column) exceeds about 14%. If mild softening is allowed, the reinforcement ratio must still exceed about 8%. These ratios are surprisingly high. If they are not used in design, one needs to pay attention to the localization of softening damage, accept the (deterministic) size effect engendered by it, and ensure safety margins appropriate for protecting against sudden explosive brittle collapse. This is of particular concern for the design of very large columns.

## Introduction

As is well known, the compression failure of concrete columns without strong lateral confining reinforcement is very brittle. The cause of brittleness is strain-softening damage of concrete under compression. The damage typically consists of a band of axial splitting microcracks which does not form over the whole cross section of a column simultaneously but propagates during failure laterally (Bažant and Xiang 1997; Bažant and Planas 1998). Since the compressive stress is reduced by the band of microcracks, the zones adjoining the band are getting unloaded during propagation and the stored strain energy released by unloading drives the propagation. The rate of energy release increases with the structure size, which causes the brittle compression failure to exhibit a size effect, i.e., the larger the column, the lower is the average stress in the column cross section at ultimate load.

To capture these phenomena, the column must be analyzed according to the energy release criteria of fracture mechanics. The only way to avoid them, as is well known, is to subject concrete to lateral confinement by a sufficiently strong circular steel tube or spiral. The question is, how strong. In mechanics terms, this leads us to ask:

*What is the minimum lateral confinement needed to completely suppress postpeak softening of the load-deflection diagram and thus eliminate the size effect?*

This vital question has not yet been answered. The answer to this question, which is sought in this paper, is proposed to serve as an objective rational criterion for the design of column confinement.

The answer cannot be obtained on the basis of the current codified approach to the design of reinforced concrete columns. The current design practice relies on the plastic limit design philosophy, which is inapplicable when the load-deflection diagram exhibits postpeak softening. This current practice ignores the fact that, due to propagation of strain-softening damage, the material strength at different points of the cross section does not get mobilized at the same time, and that the progressive nature of collapse gets more pronounced as the column size increases.

The answer to the foregoing question must be obtained by a detailed simulation of the damage process and supported by suitable experiments. The so-called ''tube-squash'' test developed by Bažant et al. (1999) and analyzed by finite elements by Brocca and Bažant (2001a), may be used for the present purpose. In this test, concrete-filled tubes are squashed to about one half of their original length and allowed to bulge laterally. Conducting tests for various tube thicknesses, one can extract information on the effect of various levels of confinement.

A realistic nonlinear triaxial constitutive model with strain-softening damage must be employed to analyze and interpret the tube-squash tests. To simulate the behavior of concrete in the tube, the latest version of the microplane constitutive model labeled as version M4 (Bažant et al. 2000a,b; Caner and Bažant 2000), is used, and the geometrical nonlinearity of large strains is taken into account. Model M4, including its large-strain version, was originally developed for simulating the penetration of missiles into concrete walls and the ground shock effects on buried

[1]Assistant Professor, Mustafa Kemal Univ., İnşat Mühendisliği Bölümü, T. Sökmen Kampüsü, 31027 Antakya, Turkey; formerly, Graduate Research Assistant, Northwestern Univ., Evanston, IL 60208.

[2]McCormick School Professor and Walter P. Murphy Professor of Civil Engineering and Materials Science, Northwestern Univ., Evanston, IL 60208. E-mail: z-bazant@northwestern.edu

hardened structures (Bažant et al. 2000b). The model has been calibrated and verified by numerous test data for the most basic types of tests (Caner and Bažant 2000).

The steel in the tube is simulated by a microplane model as well. This model (Brocca and Bažant 2001a,c) is equivalent to the classical hardening $J_2$ plasticity for the case of proportional (radial) loading paths. However, unlike that classical theory, this model can correctly reproduce the vertex effect for nonproportional loading paths with principal axes rotating against the material. This is a very important effect in the case of great deviations from proportional loading, which characterize the large deformations of the steel tube. Although this effect was brought to light long ago by the tests of Gerard and Becker (1967), the vertex effect has generally been ignored in finite-element simulations with constitutive models such as the $J_2$ plasticity, expressed in terms of tensors and their invariants. Such models miss the vertex effect.

The finite strains that occur in the steel tube are handled in step-by-step loading by the updated Lagrangian approach (e.g., Zienkiewicz and Taylor 1991; Crisfield 1997). A special finite-strain formulation of the microplane constitutive law, combining nonconjugate Green's Lagrangian strain and back-rotated Cauchy stress, is used for concrete (Bažant et al. 2000a). The reason is that, among all strain measures, Green's Lagrangian strain tensor is the only one for which the resolved strain vector on the microplane fully defines the stretch and shear angle on that plane, and that, among all the stress tensors referred to the initial (undeformed) configuration, the back-rotated Cauchy stress is the only one for which the resolved stress vector on the microplane fully defines the forces acting on that microplane. For a detailed justification and demonstration that the laws of thermodynamics are not violated, see Bažant et al. (2000a).

After verifying and calibrating the finite-strain finite-element code by the tube-squash tests, the same computer code will further be applied to tubular columns with other wall thicknesses, to long (nonbulging) sections of tubular columns, and to spiral columns.

Aside from the fracture mechanics aspects of postpeak behavior and size effect, a major progress in the understanding of load capacity of tubular concrete-filled columns has been achieved during the last several decades, beginning with Furlong (1967). For a detailed historical account, see Schneider (1998), who found slender tubular columns to lack composite action and show little or no improvement in ultimate strength, while short columns did exhibit composite action and improved ultimate strength. Roeder et al. (1999) studied the bond between the concrete core and the steel tube in columns in which all the axial load was applied on the core so as to produce slip against the confining tube. They found the average bond strength to vary between 0.5 and 3.25 MPa for diameter-to-wall thickness ratios $D/t < 50$. Schneider (1998) also analyzed the effect of steel wall thickness on column yield strength and concrete core confinement, using the orthotropic material model for concrete from the theory manual for version 4.8 of the commercial finite-element code ABAQUS (1989). This is an associated elastic-plastic model using a simple form of yield surface of Mohr-Columb type written in terms of the first two invariants of the stress tensor. However, this and other models of the classical plasticity type are not realistic, especially not for very high-confining pressures and highly nonproportional loading with vertex effects due to rotating principal stress axes.
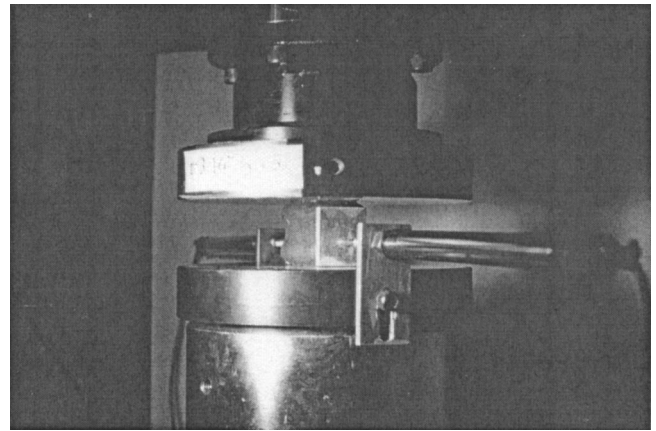


**Fig. 1.** Test setup for axial compression of specimens, showing on two sides linear variable differential transformers (LVDT gauges)

## Experimental Investigations

The results of the previously reported (Bažant and Planas 1998) tube-squash tests with steel wall thickness of $t = 12.7$ mm (0.5 in.) were used as a part of the data base in the present study. These previous tests were complemented by further similar tests of otherwise identical specimens with tubes of two different smaller wall thicknesses $t$, No. 1 with $t = 4.76$ mm (3/16 in.) and No. 2 with $t = 1.59$ mm (1/16 in.). For all the three thicknesses, the tubes had the same inner diameter $D = 38.1$ mm (1.5 in.) and the same length $L$ 88.9 mm (3.5 in.). The steel ratios $\rho$ corresponding to these three wall thicknesses were 64.0, 36.0, and 14.8% ($\rho$ = ratio of the steel area to the combined area of steel and concrete in the cross section, in the initial undeformed configuration). The tubes were made of a highly ductile steel alloy ASTM No. 1020 with Young's modulus $E = 46,852$ MPa (6,800 ksi) and Poisson's ratio $\nu = 0.25$. The filling of the tubes was a normal strength concrete with maximum aggregate size of 9.52 mm (0.375 in.), uniaxial compressive strength $f'_c = 41.37$ MPa (6 ksi), and Young's elastic modulus $E = 24,115$ MPa (3,500 ksi); its Poisson's ratio is taken as $\nu = 0.18$. The larger size aggregates used in concrete consisted of dolomite, granite, and basalt with traces of schist. River sand (No. 2 sand) and Type I Portland cement were used. Filled with concrete, and ends without sealing, the specimens were cured in a fog room for 28 days.

The concrete-filled tubes were compressed axially under displacement control in a servo-controlled closed-loop MTS testing machine until the steel tube fractured, which happened when the tube length was reduced to about one half. This custom-built machine had an extremely stiff frame with a load capacity of 4.448 MN (one million pound), although the highest load needed to squash the specimens No. 1 was only 18% of this value. The specimens were loaded at a constant axial displacement rate of 0.0254 mm/s (0.001 in./s). By virtue of very strong confinement in the steel tube, shear angles over 70° and axial compressive strains of the order of 50% were achieved in concrete without any breakup (Bažant et al. 1999).

Fig. 1 shows the test setup. The axial forces and displacements along with the maximum lateral expansions of the steel tube are recorded during the test. Linear variable differential transformers (LVDTs), visible on the sides of the specimen, were used to measure deformations (their range was ±25.4 mm or ±1 in.). After the experiment, some of the specimens have been cut into two halves axially and inspected visually for damage distribution in
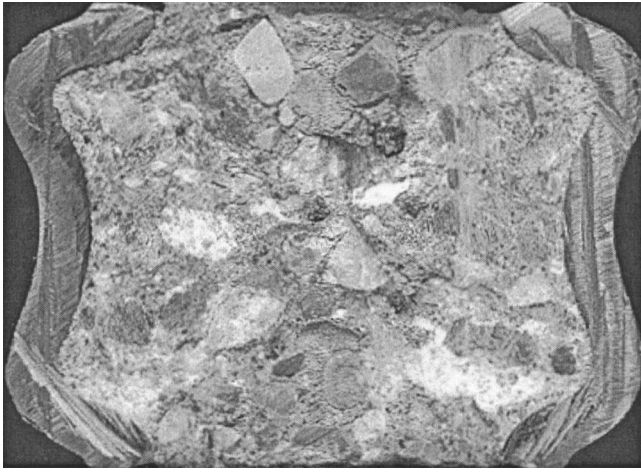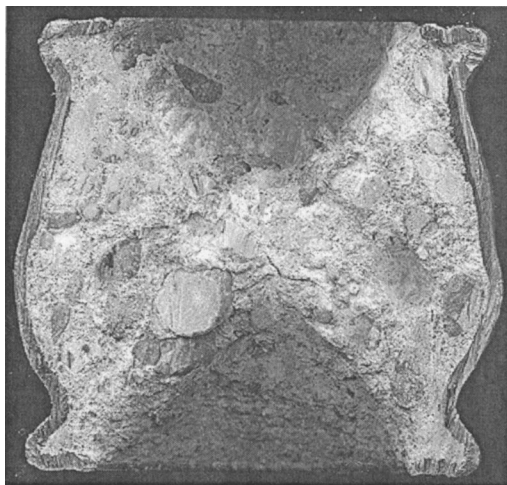
**Fig. 2.** Typical specimen of type No. 1 cut axially after experiment for visual inspection and digitization of its cross-section geometry



**Fig. 4.** Determination of critical wall thickness of steel tube using experimental data points on minimum effective tangential stiffness in axial direction observed in test (point marked Kim's is taken from Bažant and Planas 1998

the concrete core. Figs. 2 and 3 show the cut sections of specimens No. 1 and No. 2 after the test. In specimens of type No. 1 (thicker wall), no softening damage (cracking) is visually detected, except for a barely discernible shear band initiating from the loading platen. On the other hand, in specimens No. 2 (Fig. 3), completely developed shear bands are observed, and the concrete close to the steel around the midsection of the specimen is seen to have suffered microcracking.
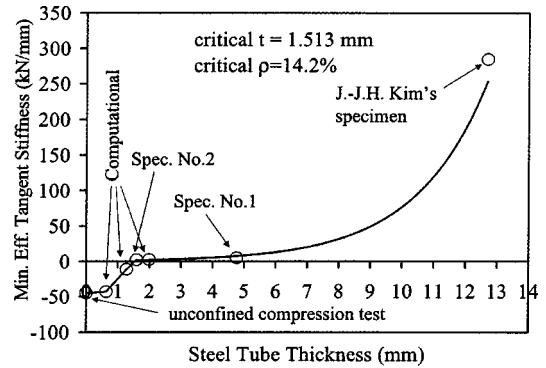
## Finite-Element Analysis with Microplane Model

The finite-element analysis of the axisymmetric problem is performed using an explicit dynamic finite-element driver which was originally developed by Brocca and Bažant (2001a,c) (since the problem is static, the technique of dynamic relaxation is applied). Because the steel is subjected to very large strains, the finite-element driver is coded using the updated Lagrangian formulation.

Based on examining the axial cuts of deformed specimens, a perfect contact with no slip is assumed to exist between the speci-



**Fig. 3.** Typical specimen of type No. 2 cut axially after experiment for visual inspection and digitization of its cross-section geometry

men and the loading platens. On the other hand, the cuts show a slip between the deforming tube and concrete at the interface. Separation is seen to occur as well—at the highly curved concave folds of the inner-tube surface. Besides, separation from the inner-tube surface must also occur during initial elastic loading because the steel tube has a much higher Poisson ratio (0.25 compared to 0.18). The slip and separation are modeled by inserting into the finite-element mesh a very thin layer of transversely isotropic finite elements that have a very low-shear modulus and are very weak for tension (albeit not for compression) in a direction normal to the interface.

The nonlinear triaxial behavior of concrete is described by microplane Model M4, which is the latest in a long sequence of microplane models developed at Northwestern University since 1983 (see Bažant et al. 2000b, with a detailed historical review). Model M4 was calibrated with a wide range of experimental data (Caner and Bažant 2000), encompassing all the basic test types in use. Model M4 has only two pairs of adjustable (free) input parameters, each of which can be easily calibrated separately, using the given values of stress and strain at a uniaxial compressive peak load and the pressure volume curve for hydrostatic loading. These input parameters, with the notation used in Caner and Bažant 2000), were identified for the present concrete as $k_1 = 0.0004$, $k_2 = 350$, $k_3 = 10$, and $k_4 = 150$.

The general idea underlying the microplane model, which was proposed by G. I. Taylor (1938) for plasticity of polycrystalline metals and is used today in various sophisticated Taylor models for metals (reviewed in Brocca and Bažant 2001c), is to characterize the material behavior not by tensors but by the stress and strain vectors acting on planes of various orientation in the material, named later (in 1984) the "microplanes." The contributions from the microplanes of all possible orientations at a given point of the material are then suitably combined to obtain the continuum response at that point. At Northwestern Univ., several new concepts were introduced to extend and adapt this idea to concrete (in detail, see Bažant et al. 2000b; Brocca and Bažant 2001c).

The strain vector on a microplane is assumed to be the projection of the continuum strain tensor $\epsilon_{ij}$. This is called the kinematic constraint between the microplanes and the continuum (and is to be distinguished from the static constraint used in the Taylor models for metal plasticity, in which microplane stress vector is the projection of the continuum stress tensor $\sigma_{ij}$). Thus, the normal and shear components of the microplane strain vector are:

$$\epsilon_N = \epsilon_{ij} n_i n_j, \quad \epsilon_L = \epsilon_{ij}(l_i n_j + n_i l_j)/2, \quad \epsilon_M = \epsilon_{ij}(m_i n_j + n_i m_j)/2 \tag{1}$$

Here, the Latin lower-case subscripts refer to Cartesian coordinates $x_i$ ($i = 1,2,3$); repeated indices imply summation; $n_i$ unit normal to the microplane; $\epsilon_L, \epsilon_M$ = shear strains on the microplane in the directions of two mutually orthogonal unit vectors $\vec{l}$ and $\vec{m}$ both normal to $\vec{n}$, which are generated in advance (randomly, to minimize the directional bias). It is useful to also introduce $\epsilon_V = \epsilon_{kk}/3$ = volumetric strain for small strains, which is the same for all microplanes. While a static constraint has been used from the outset in the Taylor models for hardening plasticity of metals (Brocca and Bažant 2001c), the kinematic constraint was introduced for concrete in 1984 because it was found necessary for ensuring model stability when strain softening takes place.

A volumetric-deviatoric split of the microplane constitutive relation is introduced by setting

$$\epsilon_N = \epsilon_D + \epsilon_V \tag{2}$$

where $\varepsilon_V$ = volumetric strain. One purpose of this split is to capture the fact that uniaxial compression tests terminate with softening while hydrostatic and perfectly confined compression tests do not, and another purpose is to achieve the full thermodynamically admissible range ($-1, 0.5$) of Poisson's ratio. For the microplane stresses, the analogous volumetric-deviatoric split, $\sigma_N = \sigma_D + \sigma_V$, is valid only for the linear elastic range, in which the elastic response is defined on the microplane level as

$$\sigma_D = E_D \epsilon_D, \quad \sigma_V = E_V \epsilon_V, \quad \sigma_L = E_T \epsilon_L, \quad \sigma_M = E_T \epsilon_M \tag{3}$$

where $\epsilon_N$, $\epsilon_V$, $\epsilon_L$, and $\epsilon_M$ are obtained using the kinematic constraint given by Eq. (1) and $\epsilon_D$ by Eq. (2). The elastic moduli on the microplane are given by $E_D = E_T = E/(1+\nu)$ and $E_V = E/[3(1-2\nu)]$ where $E$ is Young's modulus and $\nu$ Poisson's ratio (see Bažant et al. 2000b). In the inelastic range, the constitutive laws on the microplane are defined using strain-dependent yield limits, called the stress-strain boundaries, having the general form

$$\sigma_N = \mathcal{F}_N(\epsilon_N), \quad \sigma_D = \mathcal{F}_D(\epsilon_D), \quad \sigma_V = \mathcal{F}_V(\epsilon_V),$$
$$\sigma_L = \mathcal{F}_T(\epsilon_L), \quad \sigma_M = \mathcal{F}_T(\epsilon_M), \tag{4}$$

The elastic stress increments on the microplane, as calculated from Eq. (3) are not allowed to reach beyond the corresponding stress-strain boundary given in Eq. (4). This is ensured by making a drop of stress to the boundary value at constant strain.

Finally, equilibrium of the stress tensor and the microplanes stresses is enforced in a weak sense by using the principle of virtual work over a unit hemisphere, which yields the stress tensor

$$\sigma_{ij} = \frac{3}{2\pi} \int_\Omega \left[ \sigma_D \left( n_i n_j - \frac{\delta_{ij}}{3} \right) + \frac{\sigma_L}{2}(n_i l_j + n_j l_i) \right.$$
$$\left. + \frac{\sigma_M}{2}(n_i m_j + n_j m_i) \right] d\Omega + \sigma_V \delta_{ij} \tag{5}$$

where $\delta_{ij}$ = Kronecker delta. The integration in Eq. (5) must be performed numerically. To this end, a Gaussian quadrature with a finite number of planes over a unit sphere is used. The most efficient Gaussian quadrature formula is the 21-point formula whose errors in the hardening range are not graphically discernible and in the strain-softening range lead to a scatter band of maximum width about 5% (Bažant and Oh 1986). Other less efficient formulas with higher accuracy are also available (Stroud 1971). The algorithms for the numerical implementation of this

model in the small strain range using explicit dynamic or implicit finite-element drivers were presented in Bažant et al. (2000b).

A finite-strain formulation suitable for the Model M4 was originally developed in Bažant et al. (2000a). In that formulation, the back-rotated Cauchy stress $\mathbf{s} = \mathbf{R}^T \boldsymbol{\sigma} \mathbf{R}$ and Green's Lagrangian strain $\boldsymbol{\epsilon} = (\mathbf{F}^T \mathbf{F} - \mathbf{I})/2$, which are *not* work conjugate, are introduced as the stress and strain measures, respectively ($\mathbf{F} = \mathbf{R}\mathbf{U}$ = deformation gradient, $\mathbf{R}$ and $\mathbf{U}$ are the material rotation and the right stretch tensor, respectively, and $\mathbf{I}$ = unit tensor).

The back-rotated Cauchy stress is chosen as the stress measure because it is the only stress measure referred to the initial configuration of the material that allows a physical interpretation of its components on the microplane, so that internal friction, yield limit, tensile cracking, and pressure sensitivity can have their proper physical meanings. The reason for choosing Green's Lagrangian strain as the strain measure is that it is the only strain measure whose components on a microplane suffice alone to characterize the finite shear angle and normal stretch (defined, e.g., in Ogden 1984; or Bažant and Cedolin 1991, Chap. 11) on that microplane, independently of the strain components on other microplanes. Even though these stress and strain measures are not work conjugate, nonnegativeness of the energy dissipation is ensured because (1) the stress drop to the stress-strain boundary is made in the numerical algorithm at constant strain; and (2) because the elastic part of the strain tensor is so small that it can cause no negative energy dissipation.

An important point in the finite-strain version of Model M4 is the way of calculating the volumetric strain. This strain may not be expressed as $\epsilon_V = \epsilon_{kk}/3$, because of geometrical nonlinearity. However, instead of the classical multiplicative decomposition, one may simplify analysis by introducing an additive decomposition of volumetric and deviatoric strains, with the volumetric Green's Lagrangian strain tensor defined as

$$\epsilon_V = \epsilon_0 + \epsilon_0^2/2, \quad \text{with} \quad \epsilon_0 = (J-1)/3, \quad J = \det \mathbf{F} \tag{6}$$

(Bažant 1996). The fact that makes this simplification possible is the smallness of the volumetric strain, which in concrete never exceeds 3%.

For data-fitting purposes, it is convenient (Bažant 1996) to introduce the finite strains on the microplane in such a way that their ranges be ($-\infty, \infty$) and that the normal strain possess compression-tension symmetry, as for small strains. Accordingly, the microplane normal and shear strains are redefined as

$$E_N = \ln(1 - 2\epsilon_N)/2$$
$$\gamma_{NL} = (\tan \theta_{NL})/2 = [(1 + 2\epsilon_N)(1 + 2\epsilon_L)/\epsilon_L^2 - 4]^{-1/2} \tag{7}$$
$$\gamma_{NM} = (\tan \theta_{NM})/2 = [(1 + 2\epsilon_N)(1 + 2\epsilon_M)/\epsilon_M^2 - 4]^{-1/2}$$

In this regard, the part of the small-strain algorithm given in Bažant et al. (2000b) that evaluates the stresses from the constitutive law needs to be modified for finite strains. To this end, after obtaining the microplane normal and shear strains by projecting the Green's Lagrangian strain tensor onto each microplane using Eq. (1), the microplane normal and shear strains must be calculated using Eq. (7). The microplane volumetric strain is then determined from Eq. (6). Finally, the back-rotated Cauchy stress tensor must be calculated from Eq. (5) using the nonconjugate microplane stresses evaluated from Eq. (4).

Since the microplane model for concrete is a local continuum damage model, one must, in general, either use it in the sense of the crack band model, with the proper element size determined as a material property, or introduce a nonlocal generalization (Ba-

žant and Ožbolt 1992; Bažant et al. 1996). The correctness of the element size may be verified by comparison with the experimental data for uniaxial (unconfined) compression tests.

For a short initial period of loading, strain softening always develops because the steel tube, due to its higher Poisson ratio, expands laterally more than does the concrete core. But it does so only until the inelastic volume expansion of the concrete core begins. From that moment on, the tube provides confinement to the core. The tube prevents the strain-softening zone from developing into a localized damage band running across the specimen, which would inevitably give rise to size effect. For most of the test, strain softening is suppressed by high-confining pressure, except in thin tubes. But even in that case, a specimen-crossing damage band does not develop (Bažant and Ožbolt 1992) because the specimen is too short for its interior to be unaffected by the constraining effect of friction at the ends.

Consequently, even though the finite-element size was 0.40 to 0.74 mm (which is quite small, and would generally be too small for the aggregate size used), it was not necessary to implement a nonlocal approach (of course, if the load peaked and then decreased at increasing displacement, the nonlocal approach would be requisite). That a nonlocal concept was unnecessary was verified by the fact that the computations with different element sizes gave about the same results (note that this could not have been the case if there were any pronounced localizations). Another justification is provided by the absence of size effect, which is confirmed (1) computationally, by Bažant and Ožbolt's (1992) microplane simulations of similar specimens of sizes in the ratio 1:2:4 (the smallest having the height 54 mm); and (2) experimentally, by van Mier's (1986) tests data for specimens 100-mm long, which are shown in Eq. (7) along with their fits by the present microplane model.

The steel tube was originally modeled by Brocca and Bažant (2000a) using a microplane-based model that was made equivalent for proportional loading to $J_2$ plasticity. The advantage of such a model over the classical $J_2$ plasticity is that the strong vertex effect experimentally observed in metals for highly nonproportional loading with rotating principal stress axes (Gerard and Becker 1957) can be simulated realistically. In this model, a yield surface is introduced on each microplane, as follows:

$$f = \sigma_D^2 + \sigma_L^2 + \sigma_M^2 - k^2 \tag{8}$$

where $\sigma_D = \sigma_N - \sigma_V$ and $\sigma_V = \sigma_{kk}/3$ (repeated indices imply summation). When $f \leq 0$, the response on the microplane is linearly elastic as given by Eq. (3). The microplane strain components in Eq. (3) are the projections of the strain tensor, i.e., a kinematic constraint applies. When the state of stress becomes such that $f > 0$, plastic flow occurs. The incremental effective plastic strain on each microplane is defined as

$$\Delta \epsilon_{\text{eff}}^p = \sqrt{12} \frac{k - k_y}{3 E_T + 2 E^p} \tag{9}$$

where, by data fitting, $E^p = E(0.00588 + 0.085 e^{-20\epsilon_{\text{eff}}^p})$, $k = f(\sigma_D, \sigma_L, \sigma_M) > k_y$, and $k_y$ = radius of current yield surface. When $\Delta \epsilon_{\text{eff}}^p > 0$, the yield surface expands as described by the increment

$$\Delta k = \frac{1}{\sqrt{3} E^p \Delta \epsilon_{\text{eff}}^p} \tag{10}$$

Finally, the stresses on the microplane are determined by radial return to the expanded yield surface

$$\sigma_D \leftarrow \sigma_D \left( 1 - \frac{1}{k} \frac{\sqrt{3}}{2} E_T \Delta \epsilon_{\text{eff}}^p \right)$$

$$\sigma_L \leftarrow \sigma_L \left( 1 - \frac{1}{k} \frac{\sqrt{3}}{2} E_T \Delta \epsilon_{\text{eff}}^p \right) \tag{11}$$

$$\sigma_M \leftarrow \sigma_M \left( 1 - \frac{1}{k} \frac{\sqrt{3}}{2} E_T \Delta \epsilon_{\text{eff}}^p \right)$$

The bond between the steel tube and the concrete core is not perfect. There can be separation and also tangential slip at the interface. To simulate such phenomena, a layer of transversely isotropic elastic elements, with a thickness of only 1% of the core radius, is inserted into the finite-element mesh at the interface. For axisymmetric geometry, the linearly elastic stress-strain relation for a transversely isotropic material with respect to the principal material axes can be expressed, in Voigt notation, as

$$\begin{Bmatrix} \epsilon_1 \\ \epsilon_2 \\ \epsilon_3 \\ 2\epsilon_{12} \end{Bmatrix} = \begin{bmatrix} 1/E_1 & -\nu_{12}/E_1 & -\nu_{12}/E_1 & 0 \\ -\nu_{12}/E_1 & 1/E_2 & -\nu_{12}/E_2 & 0 \\ -\nu_{12}/E_1 & -\nu_{12}/E_2 & 1/E_2 & 0 \\ 0 & 0 & 0 & 1/G_{12} \end{bmatrix} \begin{Bmatrix} \sigma_1 \\ \sigma_2 \\ \sigma_3 \\ \tau_{12} \end{Bmatrix} \tag{12}$$

For correct simulation of the observed deformed shape of the specimens as well as the measured load-displacement curve and lateral expansion, the following assumed characteristics worked well for this interface layer: $\nu_{12} = 0.18$, Young's moduli $E_1 = 24.00$ MPa (3,500 ksi) and $E_2 = 241.2$ MPa (35 ksi), and shear modulus $G_{12} = 10.22$ MPa (0.1483 ksi). Experience with data fitting suggests that the separation at the interface is not very important for simulating the present tests, but the tangential slip (modeled as a shear strain of the thin layer) is crucial.

## Determination of Critical Confining Reinforcement

The occurrence of strain softening at a point of the material, which often causes a bifurcation of the response path, is indicated by the loss of positive definiteness of the tangential stiffness tensor $\mathbf{E} = d\boldsymbol{\sigma}/d\boldsymbol{\epsilon}$ of the material (manifested by the loss of positiveness of the first eigenvalue of $\mathbf{E}$). However, checking these conditions would overtax the computer and is actually superfluous if it is known from experiments that the specimen behaves in a stable manner and the response exhibits no symmetry-breaking bifurcation. For the tube-squash tests, this can be assumed safely. In that case, the check for strain softening and stability loss can be greatly simplified; it then suffices to check only the positiveness of the effective tangential stiffness in the direction of local loading, defined by

$$E_t = \frac{\Delta \boldsymbol{\sigma} : \Delta \boldsymbol{\epsilon}}{\Delta \boldsymbol{\epsilon} : \Delta \boldsymbol{\epsilon}} \tag{13}$$

(e.g., Bažant and Cedolin 1991). If $E_t > 0$, the material is locally stable and hardening; if $E_t < 0$, it is strain softening; and if $E_t = 0$, the material is locally at the limit of stability. Note that if, on the other hand, the absence of bifurcation could not be safely assumed, one would need to check the positiveness of $E_t$ for all the possible increments $\Delta \boldsymbol{\epsilon}$ from the given state at a given point (which is equivalent to a check of positive definiteness of $\mathbf{E}$).

The purpose of encasing concrete columns in tubes is to ensure ductility. Strictly speaking, ductility is equivalent to the absence of unstable strain softening (or unstable fracture growth). Determining the minimum necessary confinement steel ratio en-
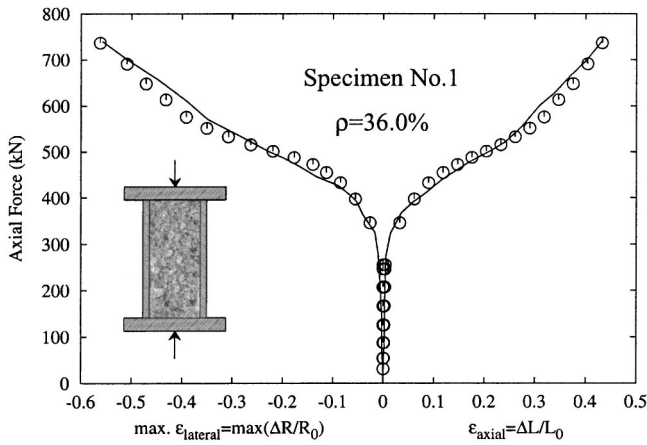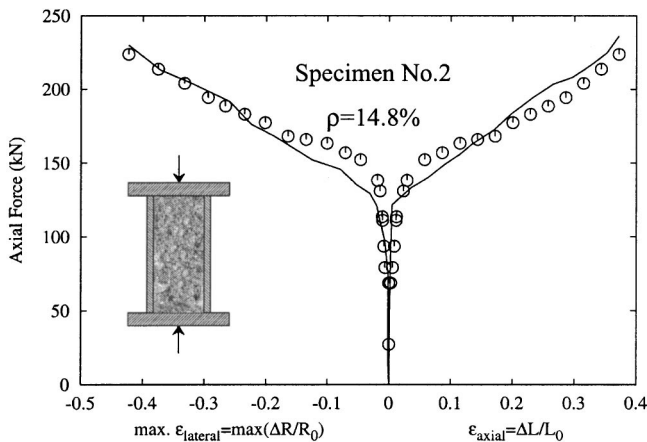
**Fig. 5.** Experimental data on axial load versus axial strain of specimen type No. 1, and their fits by finite element analysis
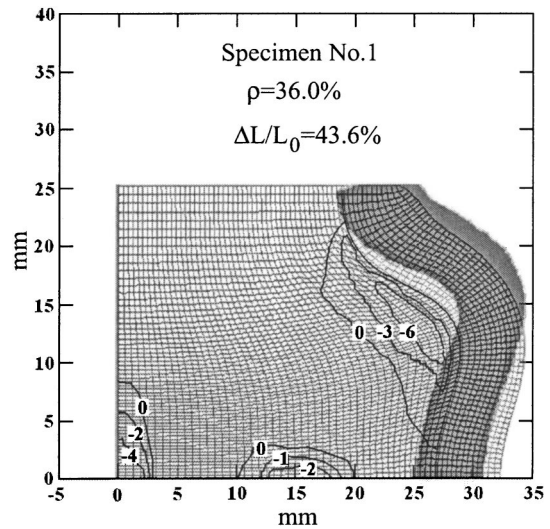


**Fig. 7.** Experimental deformed shape of typical specimen type No. 1 and its prediction by finite element analysis. Also shown are contours of equal $K_t \leq 0$

suring the absence of strain softening provides, in the strict sense, the answer to the question raised in the Introduction. Such a strict condition, however, appears reasonable only for spiral columns. It is excessively strict for tubular columns.

In tubular columns, the concrete core will always undergo limited temporary strain softening right at the start of inelastic lateral expansion of concrete, at a load much smaller than the load capacity at which the effect of local softening on ductility and strength is nil. The reason is that the higher Poisson ratio of steel will cause the elastic lateral expansion to be initially higher in the tube than in the concrete core. Therefore, it appears more appropriate to determine the critical reinforcement ratio from the condition that the load-deflection diagram would exhibit no softening.

The fitting of experimental results indicates that the proposed finite-element model simulates very well the axial load-displacement response, as shown in the Figs. 5 and 6. Furthermore, Figs. 7 and 8 show that the complex deformed shapes predicted by the finite-element calculations are quite accurate, despite the fact that a possible slip between the platens of test machine and the top or bottom surfaces of the specimen are neglected. These figures also show the contours of equal $E_t \leq 0$ normalized by Young's modulus $E$ of concrete. The contours con-

firm that the concrete rehardens after the initial temporary strain softening caused by a higher-elastic Poisson effect in steel (Fig. 9).

Having calibrated the finite-element model by experimental data, the simulations of the response for other tube thicknesses and lengths can be trusted.

The critical wall thickness $t_{cr}$ corresponding to the critical confining reinforcement ratio achieving perfect ductility may be considered as the minimum necessary to guarantee that the effective tangential stiffness $K_t$ along the response path would remain nonnegative during the entire loading.

Fig. 4 shows the minimum values of $K_t$ determined by tests as a function of steel tube thickness $t$. The plot also includes a point with negative $K_t$ which corresponds to the standard (unconfined) compression test of a cylinder ($t = 0$). This value has been calcu-



**Fig. 6.** Experimental data on axial load versus axial strain of specimen type No. 2, and their fits by finite element analysis
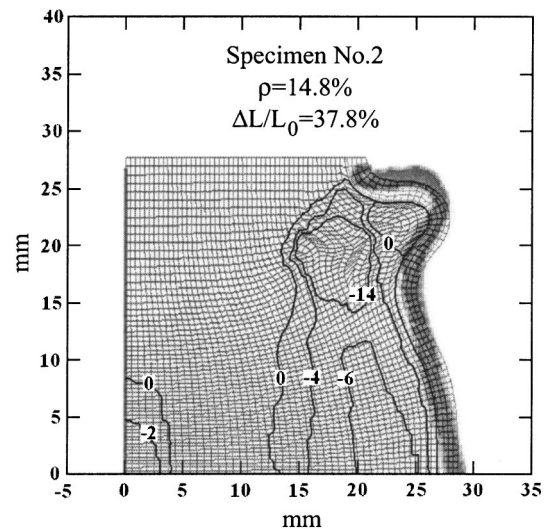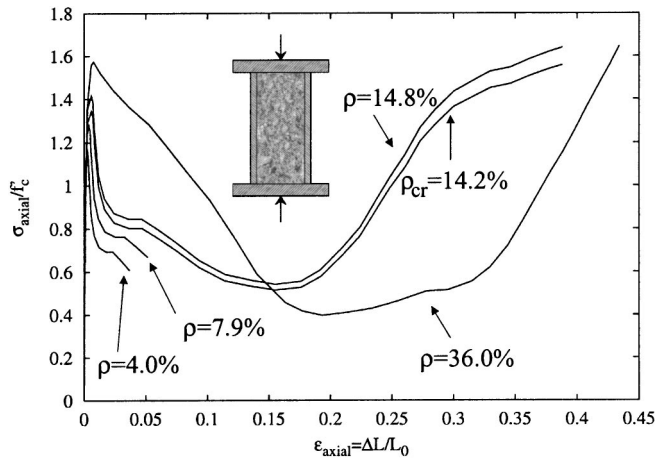


**Fig. 8.** Experimental deformed shape of typical specimen type No. 2 and its prediction by finite element analysis. Also shown are contours of equal $K_t \leq 0$ normalized by Young's modulus $E$ of concrete.

**Fig. 9.** Axial nominal stress $\sigma = F_c/A_c^0$ (normalized by unconfined compression strength $f_c' = 41.37$ MPa) versus axial strain $\epsilon = \Delta L/L_0$ of concrete during tube squash tests, as simulated by finite elements with Model M4 for different reinforcement ratios



**Fig. 10.** Axial load versus axial strain as predicted by finite element analysis with Model M4 for critical and subcritical reinforcement ratios

lated by means of Model M4. The critical thickness $t_{cr}$ for which $K_t = 0$ is seen to lie between the first two points in the plot.

The value of $t_{cr}$ might be most easily estimated by linear interpolation between the first two points; this yields $t_{cr} = 1.513$ mm, which corresponds to the critical steel ratio $\rho_{cr} = 14.2\%$. To check whether a linear interpolation is justified, two intermediate points (marked ''computational'' in Fig. 4) were calculated with Model M4. They reveal that the diagram of $K_t$ versus $t$ in the range between the first two points is curved approximately as a parabola. Using a parabolic arc to interpolate between the first two points, one gets an improved estimate of the critical thickness, $t_{cr} = 1.523$ mm, which is however nearly the same as before. This critical thickness corresponds approximately to steel ratio $\rho_{cr} = A_s/A = 14.2\%$. It may be emphasized that the experimentally determined critical thickness of the tube matches the value predicted numerically using the microplane Model M4, without any adjustment in the prediction model.

Any subcritical tube thickness will cause the load-deflection diagram of a tubular column to exhibit softening. This will cause explosive brittle response under gravity loading, and will inevitably engender a size effect.

The occurrence of softening is confirmed by the simulations with M4 of load-displacement diagrams of a tubular column element with steel ratios $\rho = \rho_{cr} = 14.2\%$, $\rho = 7.9\%$, and $\rho = 4.0\%$, shown in Fig. 10. These diagrams show that the load decrease due to softening is relatively small for steel ratio 7.9%, and so in this case the brittleness of failure and the size effect will be relatively mild. On the other hand, the load decrease is large for steel ratio 4.0%, and a high brittleness of failure and a pronounced size effect must be expected in this case.

These comparisons suggest that, in structural engineering practice, subcritical steel ratios may not cause much harm as long they are not less than roughly $0.5\rho_{cr}$. Whether the reduction factor should be 0.5 or some other value may have to be decided by the testing of full size columns.

The diagram of the average axial stress in the concrete core versus its average strain can be easily determined by separating the contributions of concrete and steel to the axial resistance of the column. The results of such separation are shown, for various reinforcement ratios, in Fig. 11. As mentioned before, regardless of the steel ratio in the tubular column, the concrete core is seen
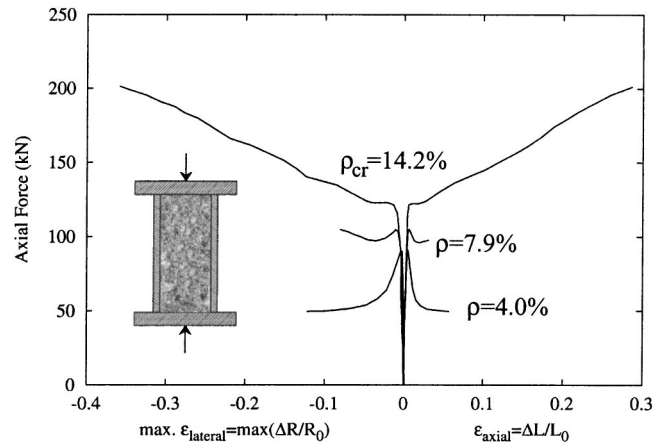
to always exhibit softening for at least a part of the loading process, because of a difference in Poisson ratios of steel and concrete. Consequently, the bond between steel and concrete gets broken early in the test and a gap develops between concrete and steel. So, the concrete is initially loaded by uniaxial stress and lacks confinement. Only after reaching its uniaxial strength, concrete expands inelastically at decreasing axial force, until a contact with the steel tube is reestablished and a large enough contact pressure is developed. It is remarkable that this does not happen until the average axial strain reaches a surprisingly large value— about 25%. Only after that, concrete begins hardening again and remains doing so for the entire test if the steel ratio exceeds the critical value. The reason that the activation of the tubular confinement requires such a large axial strain is that, after steel begins to yield, its plastic deformation occurs at constant volume, which means that the effective Poisson ratio for the yielding tube is not 0.25 but 0.5.

The softening of the concrete core cannot be eliminated, no matter how thick the tube. The only way to do so would be to make the tube from a different material, with a Poisson ratio not larger than that of concrete. This can of course be achieved with fiber composites.

## Simulations of Large Tubular and Spiral Reinforced-Concrete Columns

Having verified and calibrated the computational model, one can use it with much greater confidence to predict the behavior in similar situations. This has been done to study the response of long tubular columns that can expand without bulging, uniformly along their length, and the response of long spirally reinforced concrete columns.

For uniformly expanding tubular columns, the simulations of the response diagrams of axial load versus axial and lateral strains for different steel ratios $\rho$ are shown in Fig. 12. Note that, for this case, the critical reinforcement ratio obtained $\rho_{cr} = 16.1\%$ is slightly larger than that obtained for the fixed end test specimens. Obviously, the reason is that, in the tube-squash test, the friction under the plates helps to provide additional confinement, an effect that is missing in a long column.

Fig. 13 shows, for different steel ratios $\rho$, the computed diagram of the axial nominal stress $\sigma = F_c/A_c^0$ (with $F_c$ = axial force
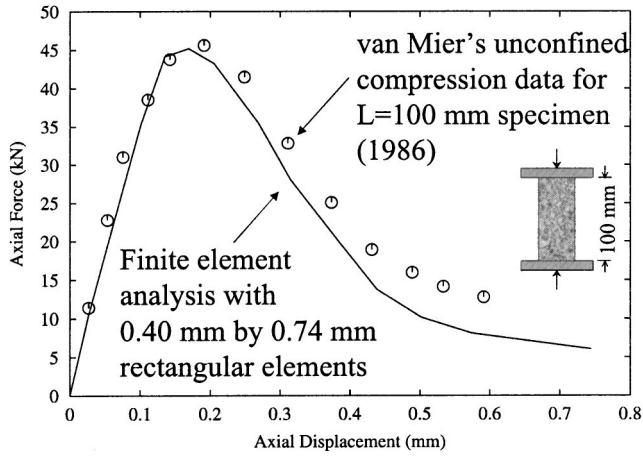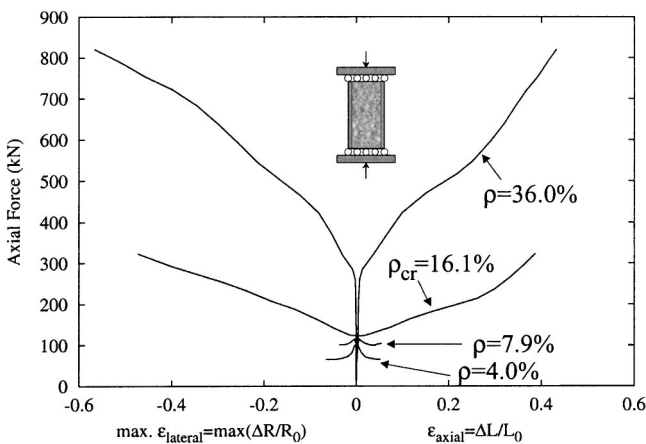
**Fig. 11.** Experimental data obtained by van Mier (1986) from unconfined compression tests with specimen length $L = 100$ mm, and its simulation using rectangular finite elements of dimensions 0.4 mm$\times$0.74 mm



**Fig. 13.** Axial nominal stress $\sigma = F_c / A_c^0$ (normalized by unconfined compression strength $f_c' = 41.37$ MPa) versus axial strain $\epsilon = \Delta L / L_0$ of concrete, as computed by finite elements for uniformly expanding tubular columns with different reinforcement ratios
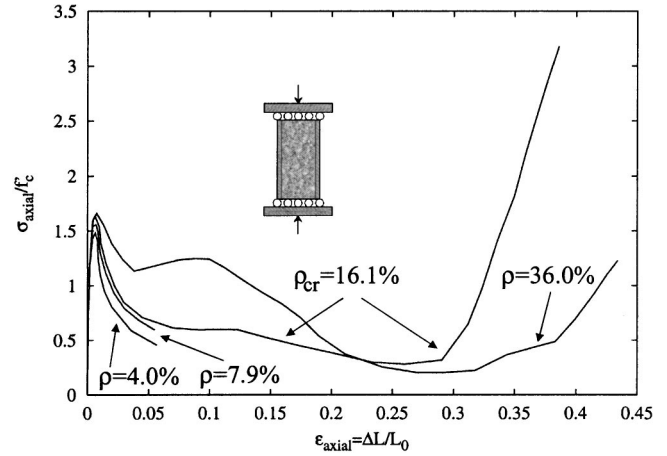
in concrete core), normalized by the unconfined (uniaxial) compressive strength $f_c' = 41.37$ MPa, versus the axial strain $\epsilon = \Delta L / L_0$ of the concrete core of a uniformly expanding tubular column. The results for different reinforcement ratios are shown. From the figure, it can be inferred that the behavior of the concrete core is very similar to that of the short tube in the tube-squash test (Fig. 9), i.e., that the effect of friction under the platens is small. The concrete core again softens during the initial stage of loading, for the same reason as already discussed.

To simulate spirally reinforced columns, their concrete cover is discounted, as is standard according to design codes. The spiral reinforcement is not modeled individually. Rather, it is assumed dense enough to be uniformly smeared, equivalent to a continuous tube consisting of an orthotropic material that has a zero stiffness in the direction of column axis. The inclination of the spiral with respect to the planes normal to the column axis is assumed small and negligible.

For programming convenience, the uniaxial stress-strain law for the spiral in the circumferential direction has been formulated by using again the microplane model for $J_2$ plasticity in a three-

dimensional finite-element simulation of the axial extension of a steel bar. The computed one-dimensional stress-strain diagram has been fit with convenient simple functions, which were then implemented in the finite-element program for the spiral column.

Fig. 14 shows the results of the uniaxial tension simulation (circular symbols) of the spiral bar and its fits by two different curves, one in the linear range and the other in the nonlinear range. The intersection of these curves, marked in the figure, is considered as the initial uniaxial yield stress.

Once this stress-strain relation for the spiral bar is available, the pressure $p$ in the concrete core produced by hoop tensile stress $\sigma$ in the spiral of current radius $R$ is readily obtained as $p = \sigma t / R$ where $t$ is the thickness of the hoop steel elements having the same volume as the spiral. From this internal pressure, the nodal forces are easily computed. The hoop strain corresponding to the hoop stress $\sigma$ according to the one-dimensional constitutive law can be computed from the radial displacements.

Fig. 15 shows the results of the finite-element simulations of spiral-reinforced columns for various reinforcement ratios $\rho$ in terms of the diagrams of the nominal axial stress versus the axial



**Fig. 12.** Axial load versus axial and lateral strains, as computed by finite elements for uniformly expanding tubular columns with various reinforcement ratios
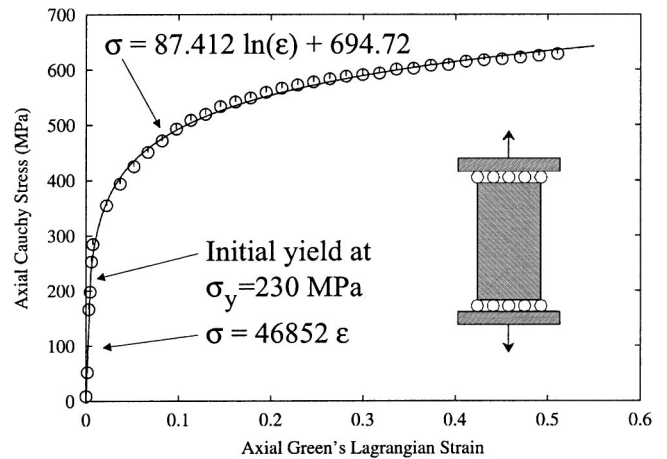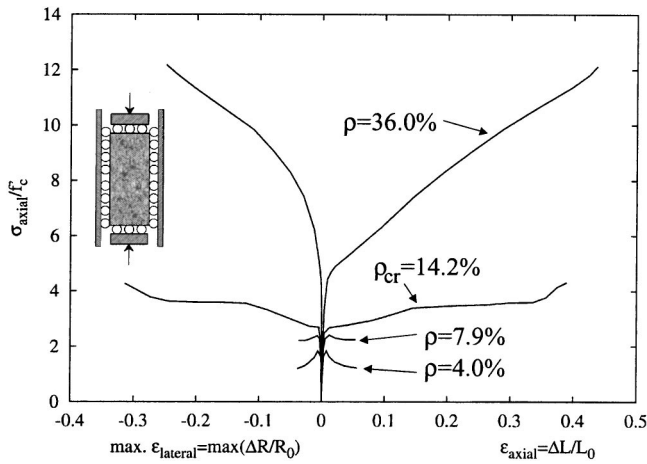


**Fig. 14.** Stress-strain diagram for confining steel in one dimension, as obtained by uniaxial tension simulation with finite elements (circular symbols), and its fits by two different curves (solid lines)

**Fig. 15.** Axial nominal stress $\sigma = F_c/A_c^0$ (normalized by unconfined (uniaxial) compression strength $f_c' = 41.37$ MPa) versus axial strain $\epsilon = \Delta L/L_0$ of concrete, as predicted by finite elements for spiral-reinforced columns with different reinforcement ratios

or lateral strain. There are two interesting points that can be inferred from this figure, namely, (1) the spirally reinforced columns with steel ratios $\rho \geq \rho_{cr}$ *never* soften, as opposed to the tubular columns; and (2) the critical reinforcement ratio $\rho_{cr} = 14.2\%$ is less than that for uniformly expanding tubular column but roughly equal to that for the tube-squash test.

As an explanation of Point 1, note the following difference between the spirally reinforced and tubular columns: As the spiral carries no axial load by itself, it does not expand due to any Poisson effect in the steel but only because the lateral expansion of concrete forces it to expand. Consequently, the concrete core is confined all the time and exhibits no initial softening.

## Conclusions and Implications for Design

1.  By performing a series of tube-squash tests on concrete-filled tubes of different wall thicknesses, it is demonstrated that a fully ductile inelastic response can be ensured only if the ratio of the cross-section area of steel to the whole cross-section area is at least $\rho_{cr} = 14\%$, which represents a critical value of the steel ratio.
2.  Verification and calibration of state-of-art material models for steel and concrete by the tube squash test makes it possible to predict the inelastic behavior of tubular and spiral columns with higher confidence.
3.  A large-strain finite-element model previously developed for the analysis of the tube-squash test is extended to handle uniformly expanding tubular columns and spiral-reinforced columns. It is found that the critical steel ratio for tubular columns is $\rho_{cr} = 16\%$, which is only slightly larger than that for the tube-squash test in which the tubes have frictional support under the platens and bulge in the middle.
4.  The concrete core of tubular columns always softens prior to large inelastic lateral expansion. This is explained by the Poisson effect, causing that the expansion of the compressed tube to be initially larger than that of concrete core. The concrete core in this type of column does not harden until the average axial strain exceeds 25%.
5.  For spirally reinforced columns, the critical steel ratio is found to be $\rho_{cr} = 14\%$, which is about the same as that for

the tube-squash test. Furthermore, it is shown that for $\rho \geq \rho_{cr}$, the concrete core confined by the spiral reinforcement *never* softens, except locally.

6.  The aforementioned minimum steel ratios needed to completely prevent softening response, i.e., to achieve plastic behavior, are significantly higher than the steel ratios currently used in design. If mild softening is allowed, the required steel ratio is roughly half as large (about 8%), which is still distinctly higher than the steel ratios currently in use.
7.  The results imply that, for the currently used steel ratios, plastic-limit analysis is not the best design concept. If the steel ratios used in designing tubular and spiral columns are not increased, one needs to pay attention to the localization of softening damage, accept the size effect engendered by it, and ensure safety margins high enough for protecting against explosive brittle behavior. This is of particular concern for very large columns.
8.  A disadvantage of the steel tube is that it separates from concrete filling. A disadvantage of spiral is that it does not carry a part of the axial load. An orthotropic fiber composite tube with a negligible Poisson ratio is free of both disadvantages, and thus represents a better design.

## References

ABAQUS *Theory Manual*. (1989). Hibbitt, Karlsson, and Sorensen, Pawtucket, R. I.

Bažant, Z. P. (1996). ''Finite strain generalization of small-strain constitutive relations for any finite strain tensor and additive volumetric-deviatoric split.'' *Int. J. Solids Struct.*, 33(20–22), 2887–2897 (special issue in memory of Juan Simo).

Bažant, Z. P., Adley, M. D., Carol, I., Jirásek, M., Akers, S. A., Rohani, B., Cargile, J. D., and Caner, F. C. (2000a). ''Large-strain generalization of microplane model for concrete and application.'' *J. Eng. Mech.*, 126(9), 971–980.

Bažant, Z. P., Caner, F. C., Carol, I., Adley, M. D., and Akers, S. A. (2000b). ''Microplane model M4 for concrete. I: Formulation with work-conjugate deviatoric stress.'' *J. Eng. Mech.*, 126(9), 944–953.

Bažant, Z. P., and Cedolin, L. (1991). *Stabilities of structures: Elastic, inelastic, fracture, and damage theories*, Oxford University Press, New York.

Bažant, Z. P., Kim, J.-J. H., and Brocca, M. (1999). ''Finite strain tube-squash test of concrete at high pressures and shear angles up to 70 degrees.'' *ACI Mater. J.*, 96(5), 580–592.

Bažant, Z. P., and Ožbolt, J. (1992). ''Compression failure of quasibrittle material: Nonlocal microplane model.'' *J. Eng. Mech.*, 118(3), 540–556.

Bažant, Z. P., and Oh, B.-H. (1986). ''Efficient numerical integration on the surface of a sphere.'' *Zeitschrift für angewandte mathematik und mechanik* (ZAMM, Berlin), 66(1), 37–49.

Bažant, Z. P., and Planas, J. (1988). *Fracture and size effect in concrete and other quasibrittle materials*, CRC, Boca Raton, Fla.

Bažant, Z. P., Xiang, Y., and Prat, P. C. (1996). ''Microplane model for concrete. I.: Stress-strain boundaries and finite strain.'' *J. Eng. Mech.*, 122(3), 245–254.

Bažant, Z. P., and Xiang, Yuyin. (1997). ''Size effect in compression fracture: Splitting crack band propagation.'' *J. Eng. Mech.*, 123(2), 162–172.

Brocca, M., and Bažant, Z. P. (2001a). ''Microplane finite element analysis of tube-squash test of concrete with shear angles up to 70°.'' *Int. J. Numer. Methods Eng.*, in press.

Brocca, M., and Bažant, Z. P. (2001b). ''Size effect in concrete columns: Finite-element analysis with microplane model.'' *J. Struct. Eng.*, 127(12), 1382–1390.

Brocca, M., and Bažant, Z. P. (2001c). ''Microplane constitutive model and metal plasticity.'' *Appl. Mech. Rev.*, 53(10), 265–281.

Caner, F. C., and Bažant, Z. P. (2000). "Microplane model M4 for concrete. II: Algorithm and calibration." *J. Eng. Mech.,* 126(9), 954–961.

Crisfield, M. A. (1997). *Non-linear finite element analysis of solids and structures, Vol. 2, Advanced topics*, Wiley, New York.

Furlong, R. W. (1967). "Strength of steel-encased concrete beam-columns." *J. Struct. Div., ASCE,* 93(5), 113–124.

Gerard, G., and Becker, H. (1957). "Handbook of structural stability. Part I: Buckling of flat plates." *NACA Tech. Note No. 3781*.

Ogden, R. W. (1984). *Non-linear elastic deformations*, Ellis Horwood, Chichester, U.K.

Roeder, C. W., Cameron, B., and Brown, C. B. (1999). "Composite action in concrete filled tubes." *J. Struct. Eng.,* 125(5), 477–484.

Schneider, S. P. (1998). "Axially loaded concrete-filled steel tubes." *J. Struct. Eng.,* 124(10), 1125–1138.

Stroud, A. H. (1971). *Approximate calculation of multiple integrals*, Prentice-Hall, Englewood Cliffs, N.J.

Taylor, G. I. (1938). "Plastic strain in metals." *J. Inst. Met.,* 62, 307–324.

van Mier, J. G. M. (1986). "Multiaxial strain-softening of concrete. Part I: Fracture, Part II: Load histories." *Mater. Struct.,* 111(19), 179–200.

Zienkiewicz, O. C., and Taylor, R. L. (1991). *The finite element method, Vol. 2, Dynamics and non-linearity*, McGraw-Hill, New York.